DOI 10.1007/s11141-023-10210-w
Radiophysics and Quantum Electronics, Vol. 65, No. 4, September, 2022
(Russian Original Vol. 65, No. 4, April, 2022)

MICROWAVE RESPONSE TO THE SYMMETRIC FAST MAGNETOSONIC WAVE

E. G. Kupriyanova,[1,2] * **T. I. Kaltman,**[3]
V. M. Nakaryakov,[2,3] **D. Yu. Kolotkov,**[2,4] **and**
A. A. Kuznetsov [2,5]

UDC 523.985

We study the observed response of microwave radiation to the perturbation of a transversely inhomogeneous plasma slab, which is stretched along a uniform magnetic field, by a symmetric (sausage-mode) fast magnetosonic wave guided by the slab. Two-dimensional modeling was carried out within the framework of the analytical solution of a system of linearized magnetohydrodynamic equations. The accelerated electrons filling only part of the slab were considered as the source of gyrosynchrotron radiation. It is shown that for gyrosynchrotron sources with a transverse size significantly smaller than the slab width and for all angles of sight there is enhancement of the microwave response to a fast magnetosonic wave. Namely, the modulation depth of the radiation is an order of magnitude higher than the initial wave amplitude, while an opposite effect was detected for gyrosynchrotron sources larger than the slab width. Contrast of the modulation depth of the radiation from narrow and wide sources increases with increasing difference of the densities outside and inside the slab. It was found that the microwave response of the slab to a fast magnetosonic wave is nonlinear, which may lead to a complete disappearance of the periodic response or its frequency doubling for certain combinations of the model parameters.

1. INTRODUCTION

Pulsed energy release in the solar corona can serve as a trigger for magnetohydrodynamic (MHD) waves of various types, and plasma inhomogeneities in the magnetic field can be waveguides for them [1, 2]. The geometry of such inhomogeneities is very diverse. Individual plasma loops that shape the coronal active regions are described by the model of a straight cylinder [1, 2]. Spicules and coronal holes are associated with open funnel-shaped configurations of the magnetic field [3, 4]. A number of inhomogeneities have a flat geometry and include a variety of current sheets with irregularities around them, as well as streamers and pseudo-streamers [5]. In addition, the arcade structure in a two-ribbon flare can be considered as a curved layer stretched along the neutral line. Propagating in the waveguide, MHD waves change the density and magnetic field of the latter, which, in turn, leads to modulation of the radiation observed in different ranges of the electromagnetic spectrum.

In particular, the manifestations of traveling fast magnetosonic (FMS) waves of radial symmetry (fast wave trains) were first detected in the decimeter radio band [6] and were associated with open magnetic

* elenku@bk.ru

[1] Main (Pulkovo) Astronomical Observatory of the Russian Academy of Sciences, St. Petersburg; [2] Institute of Solar–Terrestrial Physics of the Siberian Branch of the Russian Academy of Sciences, Irkutsk; [3] St. Petersburg Branch of Special Astrophysical Observatory of the Russian Academy of Sciences, St. Petersburg, Russia; [4] University of Warwick, Coventry, UK; [5] Irkutsk State University, Irkutsk, Russia. Translated from Izvestiya Vysshikh Uchebnykh Zavedenii, Radiofizika, Vol. 65, No. 4, pp. 287–300, April 2022. Russian DOI: 10.52452/00213462_2022_65_04_287 Original article submitted June 11, 2021; accepted February 8, 2022.

configurations. Due to the insufficient spatial but high temporal resolution of the radio instruments, these manifestations were identified for the first time by indirect signatures, namely, the characteristic appearance of a radio flux wavelet spectrum which was first obtained in [7] and named a "crazy tadpole." This kind of wavelet spectrum arises due to the group velocity dispersion during the propagation of a broadband wave packet. In this case, a narrow spectrum tail of the tadpole first appears, followed by a broadband head. Note that in the case of a plasma slab with a high density contrast, due to the non-monotonic dependence of the group velocity of a fast wave on the longitudinal wave number, the wavelet spectrum of such a perturbation takes the form of a boomerang instead of a tadpole [8]. For a monochromatic MHD perturbation, on the contrary, a sinusoidal signal is obtained (the case considered in this paper).

With the commissioning of the Atmospheric Imaging Assembly (AIA) instrument onboard the Solar Dynamics Observatory (SDO) that provides images of the Sun in the extreme ultraviolet range with a high angular resolution (0.6"), it became possible to resolve both the oscillation period and the wavelength of the FMS wave, which is impossible in the RF range. Periodic variations in the intensity of extreme ultraviolet radiation can be clearly seen in dynamic difference images and on time–distance diagrams [9, 10]. For example, in [11], it was possible to identify the radio bursts, which manifested themselves with a period slightly less than 2 min at increasingly low frequencies from 100 to 40 MHz, with traveling FMS waves having the same period as that observed before that in the SDO/AIA images. The simultaneous occurrence of wavelet tadpoles in the decimeter range and in the microwave region at frequencies of 1.1–4.5 GHz was detected in [12]. Moreover, in [13], signatures of traveling FMS waves were recorded simultaneously in the extreme ultraviolet, soft X-ray, microwave, and decimeter ranges.

The presence of accelerated electrons in plasma structures leads to the fact that the waveguide also becomes a source of radiation in the microwave range, which at frequencies above 3 GHz is usually associated with a gyrosynchrotron mechanism [14]. Due to the strong dependence of the intensity of microwave radiation on the magnitude and direction of the magnetic field in the source, weak changes in the waveguide parameters can lead to notable variations in radiation. This feature makes the pulsations of microwave radiation an effective tool for diagnosing the magnetic field in the oscillating structures of the solar corona plasma. Therefore, the study of the relation between the parameters of traveling radial FMS perturbations and the observed parameters of microwave radiation seems to be a topical problem. A similar study was performed for slow magnetosonic waves in [15]. In particular, it was shown that strong dependence of the intensity of gyrosynchrotron radiation on the density of the emitting plasma can lead to a significant, up to an order of magnitude, increase in the observed depth of radiation modulation compared with the relative amplitude of the modulating slow magnetosonic wave.

Standing axisymmetric (sausage-mode) FMS oscillations are usually observed in the microwave range in closed magnetic configurations, i. e., in separate magnetic flux tubes [16, 17] which are magnetic traps for energetic particles. Modeling of the microwave radiation response from an oscillating magnetic flux tube of cylindrical geometry was carried out in [18, 19]. It was found that for realistic amplitudes of MHD waves, the modulation depth of microwave radiation can reach tens of percent. Oscillations of the radiation intensity at different frequencies, as a rule, occur synchronously, although phase shifts may take place in certain narrow frequency intervals. Fluctuations in the intensity and circular polarization of the radiation also occur synchronously.

In these studies, it was assumed that accelerated electrons fill the entire oscillating volume. However, since the physical processes leading to particle acceleration and FMS oscillations are different, it is quite natural to expect that the localization areas of these processes do not coincide. If, during the energy release, accelerated electrons are injected not into the entire transverse thickness of the plasma inhomogeneity, but only into a part of it, then neglecting the electron diffusion effects across the magnetic field, these electrons will move only along certain magnetic field lines inside the plasma inhomogeneity. At the same time, observations show that the coronal loops, which look single due to the low spatial resolution of the radio-imaging tools, in data with a higher spatial resolution break up into a system of thinner tubes [20] oscillating as a whole [21], but each of which can serve as a microwave radiation source. Nevertheless, the effect by which not the

entire volume disturbed by the wave, but only part of it emits in the microwave range, was not studied. Therefore, the aim of this paper is to find out how the fact of mismatch of the oscillating and emitting volumes affects the microwave radiation from such a system. We limit the study to the RF range for which the gyrosynchrotron mechanism of radiation generation is relevant in solar corona conditions.

2. THE MODEL AND INITIAL EQUATIONS

We consider a waveguide in the form of a slab stretched along the z axis, the density in which varies in the transverse direction x and is constant in the longitudinal direction z. The whole system is homogeneous in the y direction. For simplicity, consider the case where an infinitely distant observer is in the xz plane. Then the three-dimensional geometry of the indicated system can be reduced to two dimensions (x and z), and the slab becomes two-dimensional. The two-dimensional slab is placed into a uniform magnetic field $\mathbf{B}_0$ so that the z axis (let us call it the waveguide axis of the slab) coincides with the field direction. In this configuration, the parallel and perpendicular components of $\mathbf{B}_0$ are equal to $B_{0z} = B_0 = \text{const}$ and $B_{0x} = 0$, respectively.

According to the formalism [22], the distribution of the unperturbed thermal-plasma density ρ_0 across the slab can be described by a continuous function obtained in the limit of the plasma parameter $\beta \to 0$ and otherwise called the Epstein profile:

$$\rho_0(x) = \rho_{\max}\mathrm{sech}^2\frac{x}{w} + \rho_\infty, \tag{1}$$

with a characteristic slab thickness w (see Fig. 1b), by which we will normalize all spatial quantities, and the density contrast

$$d = \frac{\rho_{\max} + \rho_\infty}{\rho_\infty}, \tag{2}$$

where $\rho_\infty = \rho_0(x \to \infty)$ is the plasma density at a point infinitely remote from the waveguide axis of the slab and $\rho_{\max} + \rho_\infty = \rho_0(x = 0)$ is the plasma density on the waveguide axis of the latter.

We consider the slab perturbation in the form of a traveling monochromatic symmetric FMS wave, which is generally described by a system of ideal MHD equations [see, e. g., 23, Eqs. (20)–(23)]. Such a wave in a flat layer is a counterpart of radial FMS oscillations in a cylindrical flux tube, which are also called a sausage mode. The use of ideal MHD for modeling of the wave processes in plasma inhomogeneities of the solar corona is standard (see, e. g., [1, 25]). As has been repeatedly shown, considering axisymmetric oscillations in a non-twisted magnetic cylinder or corresponding oscillations in a flat slab (without the electric current) is adequate when modeling radial FMS modes observed in the loop plasma structures of the solar corona [25]. Thus, the considered geometry is a subclass of force-free magnetic configurations.

Note that in our problem we use the flat model of plasma inhomogeneity instead of the cylindrical one. In corona physics, this approach has been used for a long time, starting with [22, 26], where it was shown that the properties of the discussed FMS waves in these systems are almost identical. With allowance for this, and since in cylindrical geometry the exact analytical solution for MHD waves, which is similar to the solution for the Epstein layer, is unknown, the flat model of plasma inhomogeneity with a transverse density profile in the form of an Epstein profile is very popular. This approach makes it possible to use the well-known analytical solution to the dispersion relation explicitly and avoid the need to join outer and inner solutions at the inhomogeneity boundary. Note also that the term “sausage mode” is employed in both the cylindrical and flat models.

In the approximation of a linear amplitudes characteristic of the solar corona, perturbations of the density and magnetic field in the wave can be expressed in terms of the plasma velocity

$$\tilde{\rho} = -\int \frac{\partial(\rho_0\tilde{V}_x)}{\partial x}\,\mathrm{d}t, \tag{3}$$

$$\tilde{B}_x = B_0 \int \frac{\partial \tilde{V}_x}{\partial z}\,\mathrm{d}t, \tag{4}$$

$$\tilde{B}_z = -B_0 \int \frac{\partial \tilde{V}_x}{\partial x}\,\mathrm{d}t. \tag{5}$$

Here, $\tilde{V}_x(x,z,t)$ is the transverse component of the perturbation velocity and t is the time. Since we have limited ourselves to considering symmetric FMS waves traveling along the z axis, the expression for $\tilde{V}_x$ can be written as

$$\tilde{V}_x(x,z,t) = AU(x)\cos[(kV_{\mathrm{ph}}t - z)], \tag{6}$$

where $A \ll 1$ is the perturbation amplitude normalized to the Alfvén velocity $C_{\mathrm{A}}(x=0)$ on the waveguide axis of the slab, k is the wave number, $V_{\mathrm{ph}} = \omega/k$ is the phase velocity of the wave, and $U(x)$ is the transverse structure of the radial FMS wave. The authors of [22] obtained an analytical solution $U(x)$ for the density inhomogeneity (1)

$$U(x) = \frac{\sinh(x/w)}{\cosh^{\zeta}(x/w)}, \qquad \zeta = \frac{|k|w}{C_{\mathrm{A}\infty}}\sqrt{C_{\mathrm{A}\infty}^2 - V_{\mathrm{ph}}^2} + 1,$$

in which the phase velocity is determined by the dispersion relation

$$\frac{|k|w}{C_{\mathrm{A0}}^2}(V_{\mathrm{ph}}^2 - C_{\mathrm{A0}}^2) - \frac{2}{|k|w} = \frac{3}{C_{\mathrm{A}\infty}}\sqrt{C_{\mathrm{A}\infty}^2 - V_{\mathrm{ph}}^2},$$

where C_{A0} and $C_{\mathrm{A}\infty}$ are the Alfvén velocity values on the waveguide axis of the slab ($x=0$) and at infinity ($x \to \infty$), respectively. Note that the solution we used corresponds to the trapped regime of the FMS wave guided by the slab. In this case, no leakage of waves from the waveguide in the direction across or obliquely to the field takes place by virtue of the total internal reflection effect.

Using Eqs. (3)–(6), we can obtain the perturbed values of the density and magnetic field of the slab:

$$\rho = \rho_0 + \tilde{\rho}, \qquad B_z = B_0 + \tilde{B}_z, \qquad B_x = \tilde{B}_x. \tag{7}$$

The distribution of the perturbed density ρ (with subtracted ρ_∞ and normalized by $\rho_{\max}$) and the distribution of the perturbed components B_z and B_x of the magnetic field (normalized to B_0) are shown by the red color scale in Figs. 1*a*, 1*c*, and 1*d*. The coordinates along the x and z axes are normalized to the characteristic width w of the Epstein profile.

3. THE SOURCE AND CALCULATION OF RADIO EMISSION

A region of finite width inside the xz layer, which is filled with non-thermal electrons with a power-law energy distribution and a an isotropic pitch-angle distribution, is considered as the source of gyrosynchrotron radiation. The region is bounded by magnetic field lines drawn symmetrically relative to the waveguide axis of the slab so that the condition of constancy of the magnetic flux between them is satisfied. In the unperturbed state, the field lines are straight lines which are parallel to the z axis and remote from it to the distance $x = |r|$, which is half the width of the gyrosynthrotron (GS) radiation source. Perturbations of the magnetic field lead to the curvature of the field lines. Using solutions $B_z(x,z)$ and $B_x(x,z)$ for perturbations of the longitudinal (z) and transverse (x) components of the magnetic field of the slab, which were obtained from Eqs. (3)–(6) for a fixed time t and wave number k, the equation of the magnetic field line $x(z)$ passing through $x = r$ at $z = 0$ can be obtained from the solution of the following first-order ordinary differential equation:

$$\frac{\mathrm{d}x(z)}{\mathrm{d}z} = \frac{B_x(x,z)}{B_0 + B_z(x,z)}. \tag{8}$$

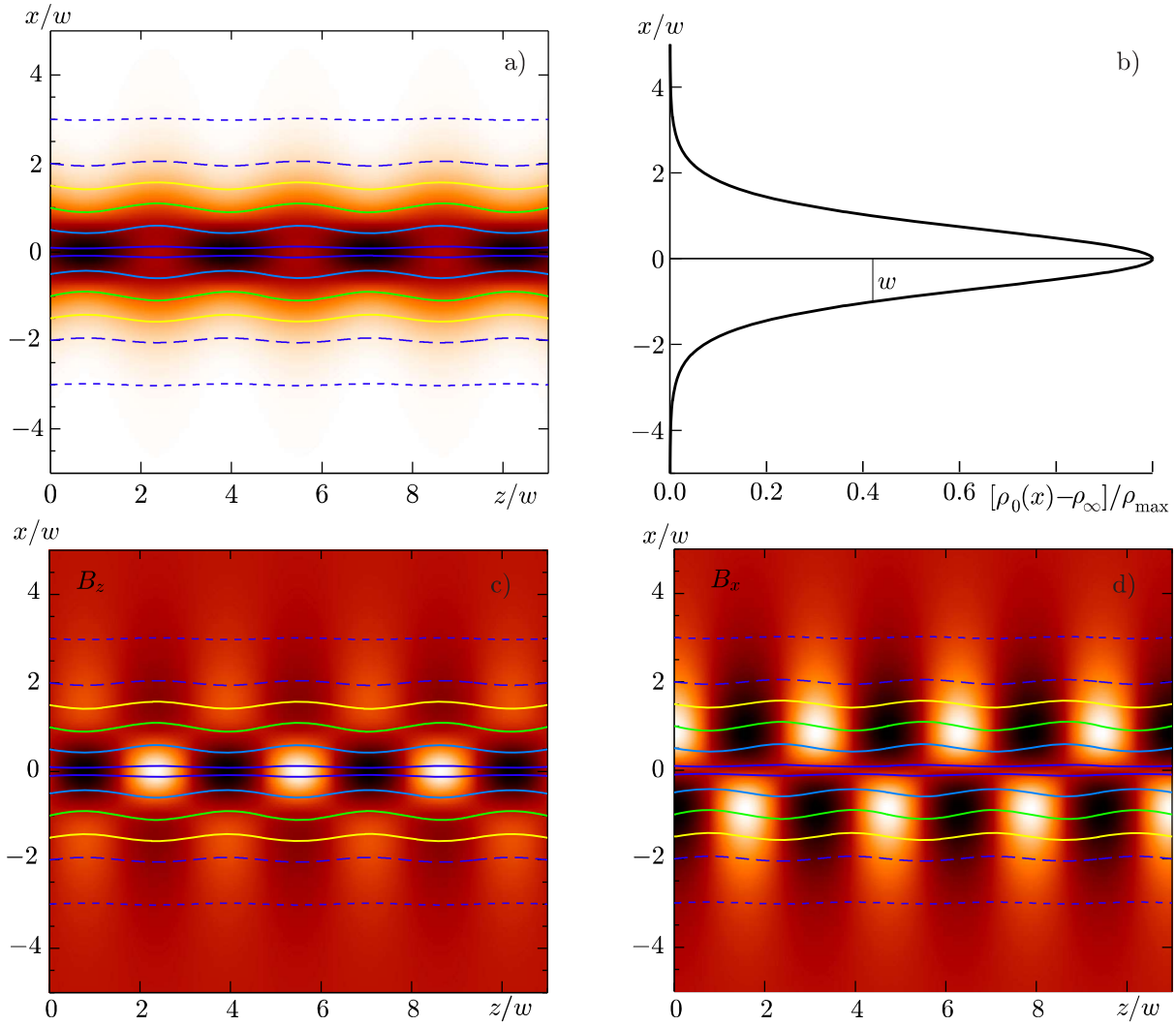

Fig. 1. Distribution of the perturbed density (*a*) and the unperturbed density with subtracted ρ_∞ and normalized to $\rho_{\max}$ in the direction of the x axis (*b*), and distributions of the perturbed components B_z (*c*) and B_x (*d*) of the magnetic field in the coordinate system of the xz layer. The darker color scale corresponds to the higher values, and the lighter colors, to the smaller values. Gyrosynchrotron sources are enclosed between pairs of magnetic field lines, shown by wavy lines of the same color and type. An example of such a source with the width $r/w = 0.5$ is given in Fig. 2.

In this paper, the solution of Eq. (8) is obtained numerically using the `dsolve` function in the Maple mathematical software package by the fourth-order Runge–Kutta method. The pairs of field lines found in this way are shown in Fig. 1 by pairs of wavy lines of different colors and types for different values of r considered in this paper. The r values also normalized to w.

A magnetohydrodynamic wave, which propagates in a slab and perturbs its parameters, affects the intensity and polarization of microwave radio emission through a change in the spatiotemporal characteristics of the medium, but does not directly modulate the process of generation of radio emission, i. e., the electron acceleration process. As an example of the relation of gyrosynchrotron radiation to the parameters of electrons and the magnetic field B, we present an approximate expression for the emissivity η of electrons distributed according to a power law in energy and isotropically in pitch angles [27]:

$$\eta \propto n_1 10^{-0.52\delta} (\sin\theta')^{-0.43+0.65\delta} B^{0.9\delta-0.22}. \qquad (9)$$

Here, δ is the spectral index, n_1 is the density of accelerated electrons, and θ' is the angle between the line of sight and the local direction of the magnetic field in the source. We denote the angle at which the observer looks at the unperturbed layer, i. e., the angle between the line of sight and the z axis of the layer as θ. The lines of sight are shown in Fig. 2*a* by straight lines of different styles for different values of the angle θ. It follows from expression (9) that with sufficiently high values of the power index ($\delta \approx 3$–4, which is typical of accelerated electrons in solar flares), the intensity of radiation from an optically thin layer strongly (and non-linearly) depends on the strength and direction of the magnetic field. It is obvious that a periodic variation in the angle and strength of the magnetic field (due to the effect of MHD waves on the medium) will also cause a periodic variation in the radiation intensity.

Exact (much more cumbersome) expressions for the emissivity and absorption coefficient of GS radiation are specified, e. g., by Eqs. (1a) and (1b) in [28]; exactly these expressions are utilized in this paper too. The algorithm for calculating the microwave radiation parameters was implemented in the form of "fast gyrosynchrotron codes" [28, 29]. Verification of this algorithm and the codes and their comparison with known analytical solutions for the GS mechanism were also performed in [28]. These codes use a specified distribution of the parameters of the radiation source (characteristics of thermal and non-thermal electrons, as well as the strength and direction of the magnetic field) along the line of sight and calculate radiation parameters by integrating the transfer equations for O- and X-mode waves, or, taking into account the direction of the magnetic field, for the right- and left-hand polarized radiation. The codes allow for the contribution of gyrosynchrotron (in the considered case, caused by non-thermal electrons) and bremsstrahlung (related to the thermal plasma) incoherent radiation mechanisms. The possible interaction of electromagnetic modes in regions with a transverse magnetic field is also taken into account [30]. Cyclotron harmonics of gyrosynchrotron radiation at low frequencies are not considered, since the integration over cyclotron harmonics is used (which significantly increases the calculation speed). In real observations, such a structure will still be smoothed due to the inhomogeneity of the source [31], as is expected.

Note that since the wavelength of the modulating MHD perturbation exceeds the wavelength of the radiated radio wave by more than 10 orders of magnitude, the problem is reduced to parametric modulation. Since in the vast majority of cases, quasi-periodic pulsations, which are considered an indicator of MHD waves in flare structures (see, e. g., reviews [32, 33]), are observed mainly in the intensity of microwave radiation, we studied the effect of MHD waves on exactly this parameter.

The intensity $I = R + L$ of microwave radiation, where R and L are the intensities of the right- and left-hand polarized radiation, respectively, was calculated in projection onto the picture plane (or the sky plane) perpendicular to the line of sight. Calculations for angles in the range $\theta = 50°$–$87°$ were performed. A transition from the coordinate system of the xz layer to the observer's coordinate system sv, where the v axis is parallel to the line of sight and the s axis lies in the picture plane, was performed. An example of orientation of the coordinate system of the slab in the observer's coordinate system for $\theta = 80°$ is shown in Fig. 2*b*.

When calculating the intensity of microwave radiation, standard parameters of the flaring loops were employed (see, e. g., [34]). The plasma temperature is assumed to be 10^7 K. The unperturbed magnetic field $B_0 = 100$ G. Plasma density in the slab is $\rho_{\max} = 3 \cdot 10^9$ cm^{-3}, and the density at infinity is obtained according to Eq. (2), $\rho_\infty = \rho_{\max}/(d+1)$, where the values $d = 10$ and 3 are chosen for flaring and quiet loops, respectively. All spatial quantities are normalized by $w = 3 \cdot 10^8$ cm.

The density of non-thermal electrons in the unperturbed layer was assumed to be constant and equal to $n_1 = 10^5$ cm^{-3}. Under the action of the FMS wave, the local distance between the field lines along the x axis changed and, accordingly, the local electron density varied in inverse proportion to that distance in order to ensure the constancy of the total particle flux (see the blue color scale in Fig. 2*a*). Calculations were carried out for non-thermal electrons distributed according to a power law in energies from 0.1 to 10 MeV with the spectral index $\delta = 3$ (see, e. g., [27]).

Note that, since the problem addressed is a model one, we consider MHD processes in the xz plane, assuming that the system is homogeneous along the y coordinate. However, to obtain the intensity values

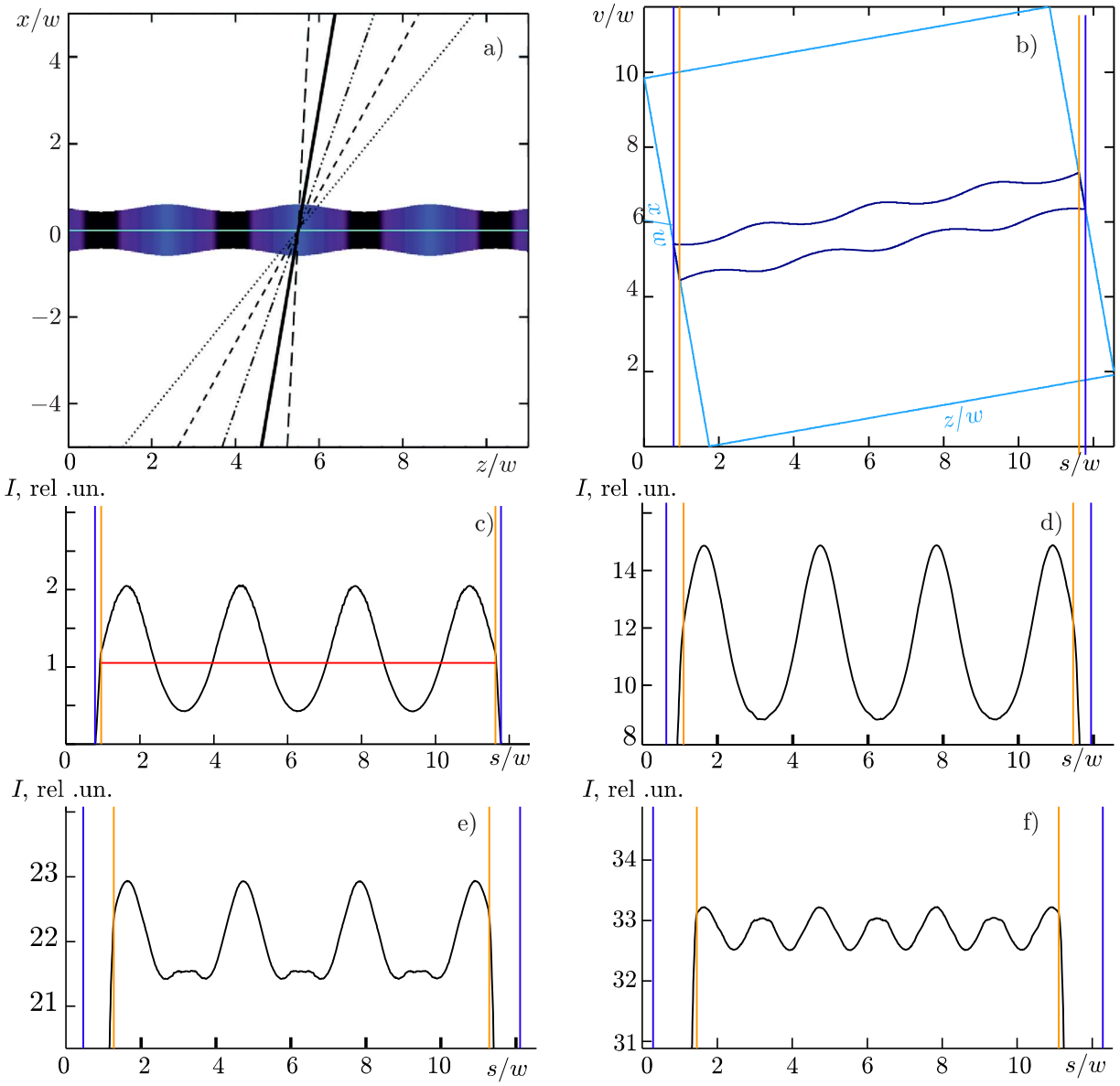

Fig. 2. (*a*) Distribution of the perturbed density of accelerated electrons in the source of GS radiation. The darker areas correspond to the higher density of accelerated electrons, and the lighter ones, to the lower density. Straight lines of different types show the lines of sight passing at different angles of sight θ. (*b*) The transition from the coordinate system of the zx layer to the observer's coordinate system sv, where the v axis is parallel to the line of sight, and the s axis lies in the picture plane. (*c*)–(*f*) Full profiles of the microwave radiation intensity at a frequency of 17 GHz in the picture plane with allowance for the contribution of the bremsstrahlung and GS mechanisms for accelerated-electron regions of different widths: (*c*) $r/w = 0.1$, (*d*) $r/w = 1.0$, (*e*) $r/w = 2.0$, and (*f*) $r/w = 3.0$ for the angle $\theta = 80°$, $A = 0.1$, and $d = 10$. Panel (*c*) shows the corresponding intensity I_0 of microwave radiation from the unperturbed layer (red line).

in solar flux units, it is necessary to specify the source size on the y axis. We took it equal to $3.6 \cdot 10^{11}$ cm. With the variation of this size, the absolute value of the intensity will change proportionally to it, but the studied characteristic properties of the radio emission will not change due to the homogeneity of the model along the y axis.

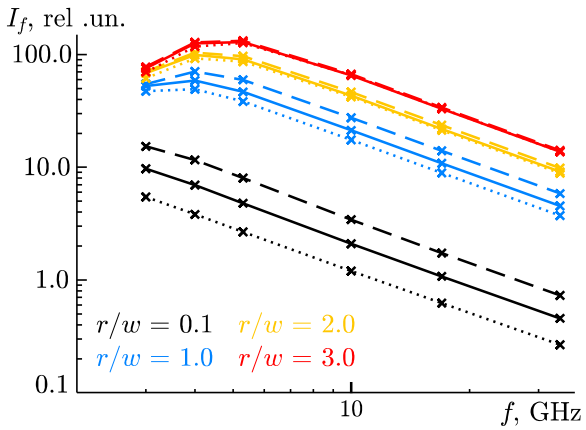

Fig. 3. The frequency spectra of the intensity I_f of microwave radiation, which were obtained by integration along the line of sight and expressed in solar flux units, as functions of the radiation frequency f for four GS sources with different transverse sizes r/w and for the model parameters corresponding to Fig. 4*a*: $A = 0.10$, $d = 3$, and $\theta = 87°$. The radiation intensity spectra of the unperturbed slab are shown by solid lines. The dashed lines correspond to the emission spectra of the perturbed layer at the intensity fluctuation maximum (see Figs. 2*c*–2*f*) and the dotted lines, at the minimum.

An example of microwave radiation spectra for different oscillation phases obtained by integration along the line of sight is shown in Fig. 3 for different widths r/w of the GS sources. The radiation intensity spectra of the unperturbed layer are shown by solid lines. The radiation spectra of the perturbed layer are shown by dashed and dotted lines. In this case, the dashed lines correspond to the positions of the intensity fluctuation maxima shown in Figs. 2*c*–2*f* and the dotted lines, to the positions of the minima. Note that the phases of the radiation intensity oscillations coincide with the phases of the FMS wave only at the angle of sight $\theta = 90°$. With the deviation from the perpendicular, different phases of the FMS wave fall into the line of sight (see Fig. 2*a*).

The intensity I profiles of microwave radiation are shown in Fig. 2 for GS radiation sources of different widths: from a narrow source ($r/w = 0.1$) in Fig. 2*c* to a wide source ($r/w = 3$) in Fig. 2*f*. The diagram shows the total intensity of the bremsstrahlung and GS radiation. Calculations show that in the considered frequency range the bremsstrahlung radiation coming from the entire region is several orders of magnitude weaker than the GS radiation coming from the region of accelerated electrons. This results in an almost zero intensity at the edges of the spatial radiation profile (between the edges of the figure and the blue vertical lines), where we see the contribution of the radiation of the thermal plasma only (see the corresponding lines in Fig. 2*b*). As soon as the field of non-thermal electrons appears on the line of sight, GS radiation starts to dominate. Its profile is bounded by orange vertical lines. As an artifact, a transition region (between the orange and blue lines), which corresponds to the boundary (triangular) areas of the region where the intensity of GS radiation is lower due to the shorter path along the line of sight, is formed. Obviously, the size of the transition region will change with a different thickness of the GS radiation source and different angles of sight. Only the central part of the profile, between the vertical orange lines, has a physical meaning.

The response of microwave radiation to variations of the slab parameters is expressed in variations in the microwave radiation intensity (see Figs. 2*c*–2*f*) and is nonlinear. A feature related to the change in the B_x component of the magnetic field arises in the slab wastes. Since the absorption coefficient of GS radiation strongly depends on the angle between the magnetic field and the line of sight, this feature of the magnetic field structure for small transverse sizes of GS sources is manifested in the flattening of the oscillation minima, which is noticeable when passing from Fig. 2*c* to Fig. 2*d*. With the further increase in transverse sizes of the source, this feature, instead of flattening, leads to the appearance of a secondary maximum (Fig. 2*e*) and, consequently, to a doubling of the number of pulsations in the observed microwave radiation (Fig. 2*f*). The profiles in Fig. 2 are plotted for $\theta = 80°$. Note that this nonlinear effect increases with increasing density contrast d. For wider GS sources, this effect becomes notable with a smaller deviation of the angle of sight from the perpendicular.

The spatial profile of oscillations transforms into a temporal one if the wave passes through a fixed point. The time scale of radiation variations is determined by the phase velocity of the wave and its wave vector: $\omega = V_{\rm ph}k$. The amplitude modulation depth of the radiation can be measured from observations as

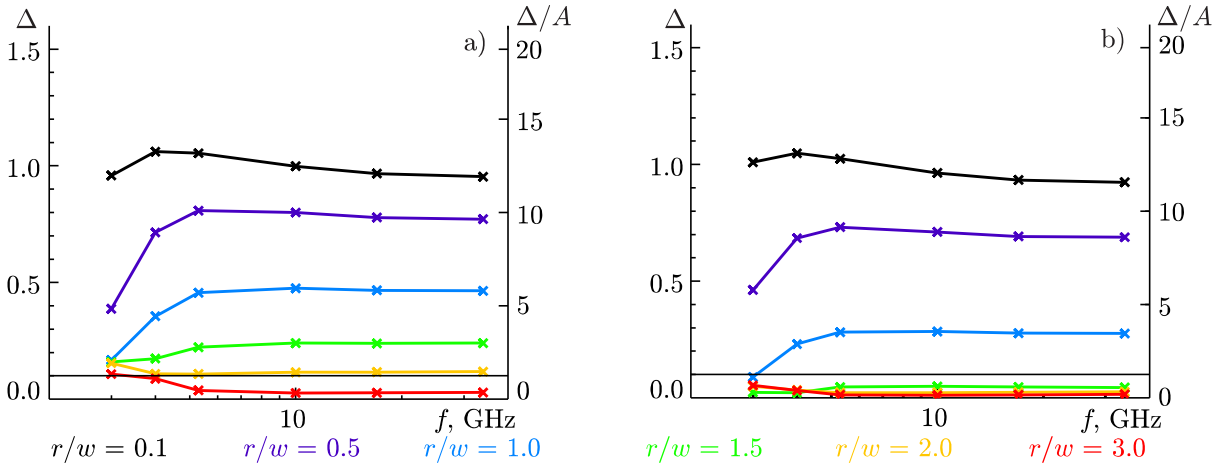

Fig. 4. Modulation depth Δ of microwave radiation at six frequencies f for the amplitude $A = 0.1$, the density contrast $d = 3$, and the angles of sight $\theta = 87°$ (*a*) and $\theta = 60°$ (*b*). Each panel shows in different colors the results for different widths r/w of the GS radiation sources. The horizontal black line shows the value of the relative amplitude A of the perturbing FMS wave.

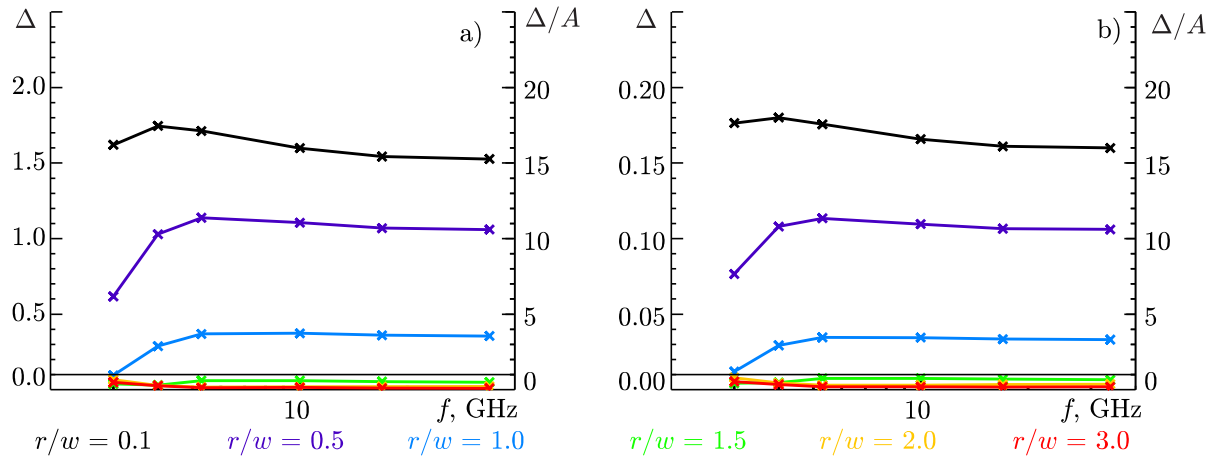

Fig. 5. Modulation depth Δ of microwave radiation at six frequencies f for different amplitudes of the FMS wave ($A = 0.1$ (*a*) and $A = 0.01$ (*b*) for the density contrast $d = 10$ and the angle of sight $\theta = 60°$. Each panel shows the results in different colors for different widths r/w of the GS radiation sources. The horizontal black line shows the value of the relative amplitude A of the perturbing FMS wave.

the difference between the maximum and minimum intensity values,

$$\Delta = (I_{\max} - I_{\min})/I_0, \tag{10}$$

with normalization by some average value of I_0. In our model case, I_0 is the intensity of microwave radiation of the unperturbed slab (e. g., the horizontal red line in Fig. 2*f*).

Comparison of the modulation depths Δ obtained for different sizes of GS sources for a low density contrast ($d = 3$) and shown in Fig. 4 by lines of different colors, and also for different angles θ, leads to the conclusion that for thin GS sources confined near the waveguide axis of the slab ($r/w = 0.1$ and 0.5), the modulation depth values are maximum and depend only weakly on the angle of sight θ. Radiation from wide GS sources ($r/w \geq 1.5$) is modulated by a wave several times weaker than for thin sources, even for angles of sight close to perpendicular, and this difference increases with the greater deviation of θ from 90°. In the case of a higher density contrast, $d = 10$ (see Fig. 5), the difference between the amplitudes is even more pronounced even for $\theta = 87°$.

Note that for GS sources of small transverse sizes ($r/w \leq 1$), a drop of the modulation depth at a frequency of 3–4 GHz compared to Δ at higher frequencies is observed. The analysis of the microwave radiation spectra (see Fig. 3) showed that with these sizes of GS sources, the spectral peak just falls on frequencies of the order of 3–4 GHz. A similar result was obtained in [35], where a decrease in the amplitude of oscillations (up to zero) was found at frequencies near the spectral maximum.

Comparison of the modulation depths Δ with the amplitude A of the perturbing symmetric FMS wave (see the Δ/A values on the right-hand vertical axis) on each panel of Figs. 4 and 5 shows that in narrow GS sources ($r/w \leq 1$), the modulation depth of the radiation is several times higher than the relative amplitude of the wave. The effect is opposite in wide GS sources: the modulation depth of microwave radiation is less than the wave amplitude, and the source thickness with which this suppression of intensity fluctuations is started depends on the angle of sight θ, the density contrast d, and the frequency of microwave radiation. This means that the wave amplitude cannot be directly estimated from the modulation depth of the intensity fluctuations of microwave radiation. This result is consistent with the results obtained in the previous studies for the radial FMS wave [19, 35] and for the slow magnetosonic wave [15].

5. DISCUSSION AND CONCLUSIONS

The aim of the work was to clarify the effect of a mismatch between the oscillating and emitting volumes on microwave radiation from such a system. For this purpose, the response of the modulation depth of the microwave radiation intensity to symmetric (sausage-mode) FMS waves, which propagate along the waveguide axis of a two-dimensional transversely inhomogeneous plasma slab stretched along a homogeneous magnetic field, was studied. Note that if a cavity is present, then reflections from its ends with the formation of a standing wave are possible. Nevertheless, traveling and standing waves differ from each other by phase shifts of plasma density perturbations and plasma flow velocity, while the modulation of GS radiation is affected by magnetic field perturbations and the density, the phase shift between which does not change during the transition from a traveling wave to a standing one. Therefore, the results obtained in this paper are also applicable to the case of a standing wave.

Any pulsed energy release, e. g., a solar flare, can serve as a trigger for MHD waves. In the problem addressed, which does not take into account the temporal nature of the trigger, the role of the flare is just to create a population of accelerated electrons and excite MHD oscillations in a waveguide that is magnetically coupled, but remote from the energy release region. This is a generally accepted effect related to the distribution of the released magnetic-field energy over microscopic and macroscopic motions (energy sink). The dependence of the properties of the generated oscillations on the temporal nature of the trigger is considered in [36].

Accelerated electrons, which are the source of GS radiation, are localized in the selected band between two magnetic field lines which are symmetric with respect to the waveguide axis of the slab. This makes our study different from the previous ones, in which accelerated electrons were considered to be distributed over the entire oscillating volume. The dependences of the modulation depth of microwave radiation on the thickness of the GS radiation sources, the angle of sight, and the contrast of densities inside and outside the slab and on the amplitude of the perturbing FMS wave were examined. It is shown that for GS sources, the width of which is less than the characteristic scale of the inhomogeneity of the thermal plasma density across the slab, an enhanced response of microwave radiation to the FMS wave is observed for all angles of sight, i. e., the modulation depth of the radiation of such a layer exceeds by an order of magnitude the relative amplitude of the perturbing wave in an optically thin region of the microwave spectrum and is several times greater in an optically thick region. The effect is opposite for GS radiation sources whose width is greater than the inhomogeneity scale of the slab: the modulation depth of the radiation is less than the relative amplitude of the wave. The observed difference between the narrow and wide sources of GS radiation increases as the density contrast is increased.

Note that in this paper we do not take into account the possible real sizes and shape of the radiation

pattern of the radio telescope, considering radiation only from selected source points with certain directions of the wave vector. To simulate the instrumental response, it is necessary to perform a convolution with the radiation pattern of a particular instrument, the size of which depends on the aperture of the instrument and the frequency band of observations. The following characteristics of instruments are important for observing the effects found in our work: (i) operating frequency in the millimeter and centimeter wavelength range and (ii) spectral, temporal, and, in prospect, high spatial resolution. This research is topical due to the planned commissioning of the largest radio interferometer Square Kilometer Array, the spatial resolution of which will be significantly higher than that of all currently existing radio instruments.

This work (including the statement of the problem, formulation and calculation of the numerical MHD model, and analysis of the results) was supported by the Russian Science Foundation (project No. 21–12–00195). Calculations of radio emission were performed by T. I. Kaltman within the framework of the state assignment to the Special Astrophysical Observatory of the Russian Academy of Sciences approved by the Ministry of Science and Higher Education of the Russian Federation.

REFERENCES

1. V. V. Zatsev and A. V. Stepanov, *Issl. Geomagn. Aéron. Fiz. Soln.*, No. 37, 3–10 (1975).
2. P. M. Edwin and B. Roberts, *Solar Phys.*, **88**, 179–191 (1983). https://doi.org/10.1007/BF00196186
3. D. B. Jess, D. J. Pascoe, and D. J. Christian, *Asrtophys. J. Lett.*, **744**, L5 (2012). https://doi.org/10.1088/2041-8205/744/1/L5
4. D. J. Pascoe, V. M. Nakariakov, and E. G. Kupriyanova, *Astron. Astrophys.*, **568**, A20 (2014). https://doi.org/10.1051/0004-6361/201423931
5. B. Decraemer, A. N. Zhukov, and T. Van Doorsselaere, *Astrophys. J.*, **893**, 78 (2020). https://doi.org/10.3847/1538-4357/ab8194
6. H. Mészárosová, M. Karlický, and J. Rybák, *Sol. Phys.*, **273**, 393–402 (2011). https://doi.org/10.1007/s11207-011-9794-6
7. V. M. Nakariakov, D. J. Pascoe, and T. D. Arber, *Space Sci. Rev.*, **121**, 115–125 (2005). https://doi.org/10.1007/s11214-006-4718-8
8. D. Y. Kolotkov, V. M. Nakariakov, G. Moss, et al., *Mon. Not. R. Astron. Soc.*, **505**, 3505–3513 (2021). https://doi.org/10.1093/mnras/stab1587
9. D. Yuan, Y. Shen, Y. Liu, et al., *Astron. Astrophys.*, **554**, A144 (2013). https://doi.org/10.1051/0004-6361/201321435
10. G. Nisticò, D. J. Pascoe, and V. M. Nakariakov, *Astron. Astrophys.*, **569**, A12 (2014). https://doi.org/10.1051/0004-6361/201423763
11. C. R. Goddard, G. Nisticò, V. M. Nakariakov, et al., *Astron. Astrophys.*, **594**, A96 (2016). https://doi.org/10.1051/0004-6361/201628478
12. H. Mészárosová, M. Karlický, J. Rybák, et al., *Astrophys. J. Lett.*, **697**, L108–L110 (2009). https://doi.org/10.1088/0004-637X/697/2/L108
13. P. Kumar, V. M. Nakariakov, and K.-S. Cho, *Astrophys. J.*, **844**, 149 (2017). https://doi.org/10.3847/1538-4357/aa7d53
14. G. A. Dulk, *Annual Rev. Astron. Astrophys.*, **23**, 169–224 (1985). https://doi.org/10.1146/annurev.aa.23.090185.001125
15. V. M. Nakariakov and V. F. Melnikov, *Astron. Astrophys.*, **446**, 1151–1156 (2006). https://doi.org/10.1051/0004-6361:20053944
16. V. M. Nakariakov, V. F. Melnikov, and V. E. Reznikova, *Astron. Astrophys.*, **412**, L7–L10 (2003). https://doi.org/10.1051/0004-6361:20031660

17. E. G. Kupriyanova, V. F. Melnikov, V. M. Nakariakov, et al., *Solar Phys.*, **267**, 329–342 (2010). https://doi.org/10.1007/s11207-010-9642-0
18. V. E. Reznikova, T. Van Doorsselaere, and A. A. Kuznetsov, *Astron. Astrophys.*, **575**, A47 (2015). https://doi.org/10.1051/0004-6361/201424548
19. A. A. Kuznetsov, T. Van Doorsselaere, and V. E. Reznikova, *Sol. Phys.*, **290**, 1173–1194 (2015). https://doi.org/10.1007/s11207-015-0662-7
20. I. V. Zimovets, S. A. Kuznetsov, and A. B. Struminsky, *Astron. Lett.*, **39**, No 4, 267–278 (2013). https://doi.org/10.1134/S1063773713040063
21. D. J. Pascoe, V. M. Nakariakov, and T. D. Arber, *Sol. Phys.*, **246**, 165–175 (2007). https://doi.org/10.1007/s11207-007-9055-x
22. T. D. Cooper, V. M. Nakariakov, and D. R. Williams, *Astron. Astrophys.*, **409**, 325–330 (2003). https://doi.org/10.1051/0004-6361:20031071
23. V. M. Nakariakov, B. Roberts, and N. S. Petrukhin, *J. Plasma Phys.*, **58**, 315–327 (1997). https://doi.org/10.1017/S0022377897005710
24. Yu. G. Kopylova, V. F. Mel'nikov, A. V. Stepanov, et al., *Astron. Lett.*, **33**, No. 10, 706–713 (2017). https://doi.org/10.1134/S1063773707100088
25. B. Li, P. Antolin, M.-Z. Guo, et al., *Space Sci. Rev.*, **216**, 136 (2020). https://doi.org/10.1007/s11214-020-00761-z
26. V. M. Nakariakov and B. Roberts, *Sol. Phys.*, **159**, 339–402 (1995). https://doi.org/10.1007/BF00686541
27. G. A. Dulk and K. A. Marsh, *Astrophys. J.*, **259**, 350–358 (1982). https://doi.org/10.1086/160171
28. G. D. Fleishman and A. A. Kuznetsov, *Astrophys. J.*, **721**, 1127–1141 (2010). https://doi.org/ 10.1088/0004-637X/721/2/1127
29. https://github.com/kuznetsov-radio/gyrosynchrotron
30. V. V. Zheleznyakov and E. Ya. Zlotnik, *Astron. Zhurn.*, **40**, 633–642 (1963).
31. A. A. Kuznetsov, G. M. Nita, and G. D. Fleishman, *Astrophys. J.*, **742**, 87 (2011). https://doi.org/10.1088/0004-637X/742/2/87
32. E. G. Kupriyanova, D. Y. Kolotkov, and V. M. Nakariakov, *Sol.-Terr. Phys.*, **6**, 3–23 (2020). https://doi.org/10.12737/stp-61202001
33. I. V. Zimovets, J. A. McLaughlin, A. K. Srivastava, et al., *Space Sci. Rev.*, **217**, 66 (2021). https://doi.org/10.1007/s11214-021-00840-9
34. V. V. Zaitsev and A. V. Stepanov, *Phys. Usp.*, **51**. No. 11, 1123–1160 (2008). https://doi.org/10.1070/PU2008v051n11ABEH006657
35. G. Mossessian and G. D. Fleishman, *Astrophys. J.*, **748**, No. 2, 140 (2012). https://doi.org/10.1088/0004-637X/748/2/140
36. C. R. Goddard, V. M. Nakariakov, and D. J. Pascoe, *Astron. Astrophys.*, **624**, L4 (2019). https://doi.org/10.1051/0004-6361/201935401